A Transient Voltage-based Approach for Mid-voltage Fault Detection through Low-voltage Sensors

Mingze ZHANG *, Xinyu GUAN, Xin AI

Posted Date: 22 March 2024

doi: 10.20944/preprints202403.1099.v1

Keywords: LV sensor measurement; non-effectively grounded system; single-phase-to-ground fault; transient aerial mode voltage

Article

A Transient Voltage-Based Approach for Mid-Voltage Fault Detection through Low-Voltage Sensors

Mingze Zhang [1,*], Xinyu Guan [2] and Xin Ai [1]

[1] School of Electrical and Electronic Engineering, North China Electrical Power University, Beijing 100096, China; 1172101058@ncepu.edu.cn.
[2] State Grid Jilin Electric Power Training Centre. Changchun 130062; 18043079595@163.com
* Correspondence: 1172101058@ncepu.edu.cn; Tel.: +86-13500996011

Abstract: Single-phase-to-ground fault in non-effectively grounded systems poses serious public safety concern. Along with increasing deployment of low-voltage (LV) sensors, new opportunities and ways are created for solving this traditional problem in distribution systems. A new approach, identifying primary single-phase-to-ground line fault and locating it through measurement data from smart sensors deployed in the secondary side of distribution transformers, is proposed in this paper. When a fault occurs in primary distribution feeder, the transient aerial mode voltage (AMV) of each LV smart sensor is calculated. The fault line can be identified by an abrupt change value of AMV at LV side. Next, by finding the position of the maximum value of this AMV from LV sensors on the fault line, the fault location can be pinpointed to two neighboring distribution transformers. The proposed method has been proven to be efficient and reliable by simulation studies.

Keywords: LV sensor measurement; non-effectively grounded system; single-phase-to-ground fault; transient aerial mode voltage

1. Introduction

For economic operation considerations, the non-effectively grounded neutral points have been adopted in the medium-voltage (MV) distribution network design in China [1]. With widespread application of such system in the grid, fault line identification and fault point location have great significance for maintaining power system reliability and ensuring network equipment safety [2,3]. Single-phase-to-ground fault is the most common fault in distribution system. When it occurs, the grounding current of distribution system goes beyond an upper limit [4], overvoltage is usually generated which endangers the insulation of distribution network and equipment [5]. More seriously, when the system operates in such a fault state, shock accident or casualties might happen [6,7], which represents a serious public safety hazard. Specifically, when a single-phase-to-ground fault occurs in non-effectively grounded system, it is difficult to be detected due to unobvious characteristics of fault current [8].

In last three decades, scholars have proposed various fault detection methods, which can be summarized as steady-state method, transient method, and signal injection method according to the different electrical signals used. Steady-state method [9–16] includes zero-sequence admittance method [9,10], zero-sequence current amplitude and phase comparison method [11–13], zero-sequence active component direction method [14], power angle method [15], negative-sequence current method [16], etc. With stable signal collection, the steady-state method has been widely used. Transient method [17–29] includes traditional energy method [17], centralized comparison method [18], wavelet analysis method [19], correlation analysis method [20], etc. It uses transient signals thus obtains abundant fault transient information and features [21]. The signal injection method includes parallel resistance method and zero-sequence current disturbance method [30–32]. This method demonstrates good ability in determining the line with persistent faults by injecting a large current

 doi:10.20944/preprints202403.1099.v1

using a dedicated or other primary equipment. Nevertheless, the above-mentioned methods all require primary feeder sensors and relevant communication capabilities for signal transmission, while the success rate of fault detection often depends on number of sensors deployed. In practice, the substantial investment required impacts the implementation of these methods, power companies often try to locate fault line through manual testing, resulting in service cut of non-fault line and down-graded power quality [33].

In recent years, the mass deployment of low-voltage (LV) sensors, especially customer smart meters and smart distribution terminals installed at LV side of distribution transformers, provides power companies with full visibility of distribution network, which also opens a new way for detecting faults on the MV side through measurement of the multiple LV sensors on this MV feeder [34–37]. In [34,35], LV voltage imbalance is compared to determine the location of faults on the MV side. Although it cannot identify short circuit faults, it performs well on detecting high impedance faults such as broken wires. In [36,37], the author proposes a LV steady-state measurement-based method, which can accurately determine the fault location after signal classification through clustering algorithm, and it works for different neutral point grounding system, but the weak change in positive-sequence and negative-sequence steady-state LV impacts its practical applications for detecting single-phase-to-grounding fault in neutral non-effectively grounded systems.

When a single-phase-to-ground fault occurs on primary feeder or the MV side of the distribution line in neutral non-effectively grounded system, the transient aerial mode voltage (AMV) changes significantly at fault moment and demonstrates a stable pattern. On non-fault lines, the AMV magnitude decreases along the line, while on the fault line it has the highest magnitude in the fault point and decreases along the feeder in both sides. Based on this, this paper proposes a new such fault detection method by monitoring and analyzing the transient signals through LV sensors. By using the AMV for fault detection, not only can the primary fault line be accurately identified, but the primary fault location can also be determined. The main contributions are as follows:

1) A novel method for monitoring single-phase-to-ground fault in MV side of the distribution network through LV sensors is proposed. The fault transient signal collected by the LV sensor is adopted for fault characteristic analysis and decision making, which demonstrate great robustness.

2) The characteristics of transient AMV at different LV sensing points after MV single-phase-to-ground fault is analyzed and derived, which enables the fault location to a reasonable range. It is found that on the non-fault line, the magnitude decreases along the feeder to the end; while on the fault line, it has the highest value in the fault point and decreases along the feeder both sides.

3) The fault line and fault location can be determined by analyzing the magnitudes of the transient AMV sensed by multiple LV sensors.

Leveraging existing LV sensors, the proposed method can be used as independent fault detection when there is no fault detection equipment on the MV side thus avoiding MV sensor capital investment, or as supplemental measure cooperating with the existing MV detection equipment. It also works for both effectively grounded system and non-effectively grounded system.

2. Fault Characteristics Analysis

In analyzing the transient process of single-phase-to-ground fault in non-effectively grounded system, the Karenbauer phase-mode transformation method, which is also known as the 1, 2, 0 transformation method, is used. The 1-mode component and the 2-mode component are collectively referred to as the aerial-mode component, and the network composed of AB phase and AC phase, respectively. The parameters are same as those of the positive-sequence network in the fault symmetric component analysis; The 0-mode component, also known as the ground-mode component, forms a network between the three-phase conductor and the earth, so it has the same parameters as the zero-sequence network in the fault symmetric component analysis [38]. For distribution transient fault signals within 3000Hz, the compound mode network of single-phase-to-ground fault through arc suppression coil (ASC) grounding system obtained by the mode transformation method, is shown as in the Figure 1 below [39].

 doi:10.20944/preprints202403.1099.v1

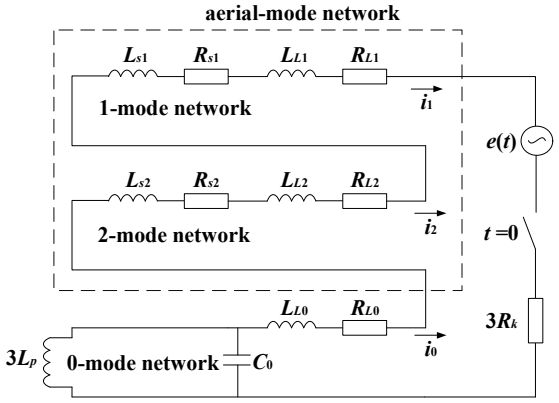

Figure 1. Compound mode network of ASC grounding system

In the figure, $e(t)$ is the power supply voltage, R_k is the grounding resistance, and L_p is the ASC inductance; L_{s1} and R_{s1} in the 1-mode network are respectively the aerial-mode inductance and resistance of the power supply system behind the bus, and L_{L1} and R_{L1} are respectively the aerial-mode inductance and resistance from the fault point of the fault line to the bus; L_{s2}、R_{s2}、L_{L2} and R_{L2} in the 2-mode network have the same meaning corresponding to 1-mode network; L_{L0} and R_{L0} are the 0-mode inductance and resistance from the fault point of the fault line to the bus, and C_0 is the sum of the 0-mode capacitance of the bus and its power source, the 0-mode distributed capacitance of all non-fault lines, and the 0-mode distributed capacitance from the fault point of the fault line to the bus, which is equal to the 0-mode distributed capacitance of the whole system minus the 0-mode distributed capacitance of the line after the fault point.

During the fault transient process, let $e(t) = U_m\cos\omega t$, ω is the power frequency, and the transient current in the compound mode network is:

$$i(t) = U_m\omega C_0\left(\frac{\omega_0}{\omega}e^{-\delta t}\sin\sqrt{\omega_0^2-\delta_0^2}\,t - \sin\omega t\right) \tag{1}$$

where $\delta = \frac{R}{2L}$ is the attenuation coefficient of resonant component, R=2(R_{s1}+R_{L1})+R_{L0}+3R_k, L=2(L_{s1}+L_{L1})+L_{L0}; $\omega_0 = \frac{1}{\sqrt{LC_0}}$ is the resonance angular frequency of the network, $U_m\omega C_0$ is the peak value of steady-state capacitive current I_c. Formula (1) can be simplified as:

$$i(t) = I_c\left(\frac{\omega_0}{\omega}e^{-\delta t}\sin\sqrt{\omega_0^2-\delta_0^2}\,t - \sin\omega t\right) \tag{2}$$

In (2), as $\delta_0 = \omega_0$, $\sqrt{\omega_0^2-\delta_0^2}$ is approximately equal to ω_0, thus ω_0 is referred to as transient dominant resonant angular frequency, and its value is generally 300~2000Hz in the distribution network [39]. When t equals to a quarter period of the transient dominant resonant frequency, $\sin\sqrt{\omega_0^2-\delta_0^2}\,t \approx \sin\omega_0 t$, and $e^{-\delta t} \approx 1$, the formula (2) can be simplified as follows:

$$i(t) = I_c\left(\frac{\omega_0}{\omega}\sin\omega_0 t - \sin\omega t\right) \tag{3}$$

In (3), the value of $\sin\omega t$ is relatively small; when $\sin\omega_0 t$ is at its peak moment, the instantaneous value of $i(t)$ is close to its maximum value, and the ratio of the peak value to the magnitude of the system steady-state capacitive current to the ground is approximately the ratio of transient dominant frequency ω_0 to power frequency ω. Generally, the ratio can reach more than ten times of the steady-state magnitude [33,39], thus this transient feature has good observability in LV measurement which can be used to detect the fault occurrence.

 doi:10.20944/preprints202403.1099.v1

It can be further known from Figure 1, at the initial stage of the transient process t = 0, the transient current is composed of capacitance charging/discharging current and inductance current. No matter how the neutral point is grounded, there is an equivalent capacitance C_0 in grounding system that affects the transient current of the compound mode network. According to formula (1), in the initial stage of the transient process, the characteristics of the transient current are mainly determined by the transient capacitive current, which is much larger than the transient inductance current. Therefore, the distribution of the transient voltage depends on the capacitance value which also determines the maximum transient voltage value. In the MV distribution system, the transient voltage value dominated by C_0 is relatively high, basically maintaining at the kilovolt level; After the transition to the steady-state, the voltage is distributed by the inductance L_p, and transits to the hundred-volt level [33,39], which is far smaller than the that in initial transient process, so it is much more reliable to detect the fault using the transient signals compared to steady signals. When a single-phase-to-ground fault occurs, with the same power source, the equivalent capacitance to the ground of the non-fault line dominates its transient AMV instantaneous value. As the distribution feeders are generally short, the capacitance to the ground of each feeder has no obvious difference, resulting in small AMV instantaneous value on the non-fault line and this value decreases along the line; The AMV instantaneous value on the fault line is determined by the capacitance of all lines to the ground, which is much larger than that of the non-fault line. Therefore, the transient fault signals on the MV side are regularly distributed along the line. The transient signal within 3000Hz has little attenuation through the distribution transformer, thus it can be transmitted to LV distribution network [39,40] and caught in the secondary side of distribution transformer. Based on the above analysis, fault on the MV feeder can be detected with LV measurements at each point of the distribution feeder.

After identifying the fault line, the location of the fault point can be further determined through the measurement data of all LV sensors on the line. Considering aerial-mode parameters of the downstream line and load at the fault point in Figure 1, the 1-model network is shown in the following Figure 2.

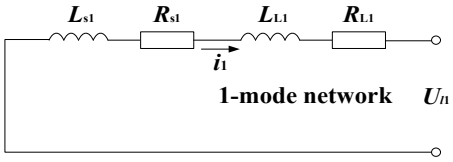

Figure 2. The mode 1 network of single-phase grounding fault.

The voltage U_{l1} of network in Figure 2 is:

$$U_{l1} = (R_{s1} + R_{L1})i_1 + (L_{s1} + L_{L1})\frac{di_1}{dt} \tag{4}$$

In (4), i_1 is the transient current. From Figure 1 and Figure 2, it can be seen that U_{l1} is the aerial-mode component of the fault transient voltage, which is the AMV value at the fault point. In order to analyze the distribution pattern of AMV along the fault line, the load side line parameters after the fault point are supplemented in Figure 2. For the convenience of analyzing, the impact of ground capacitance is ignored [41], the fault AMV distribution on a single line can be approximately represented by Figure 3.

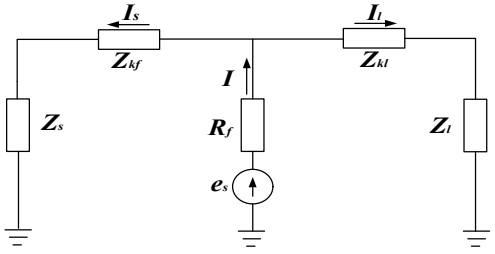

Figure 3. The fault AMV distribution

Preprints.org (www.preprints.org) | NOT PEER-REVIEWED | Posted: 22 March 2024 doi:10.20944/preprints202403.1099.v1

In the figure, e_s is the virtual power supply at the fault point, R_f and I are the aerial-mode component of grounding resistance and fault current, I_s and I_l are the power source side and load side components of I; Z_s is the system aerial-mode impedance, with value as the sum of L_{s1}, R_{s1}, L_{s2}, R_{s2} and the equivalent capacitance of the power source; Z_{kf} is the aerial-mode impedance from the bus to the fault point of the fault line, with value as the sum of L_{L1}, R_{L1}, L_{L2}, R_{L2} and the equivalent capacitance from the fault point to the bus of the fault line; Z_{kl} is the aerial-mode impedance of other parts of the fault line; Z_l is the aerial-mode impedance of the fault line load. For a more intuitive analysis of AMV distribution along the feeder, Z_{kf} and Z_{kl} are divided into several parts to represent the feeder segments marked by distribution transformer locations on the line, and the results are shown in the following Figure 4.

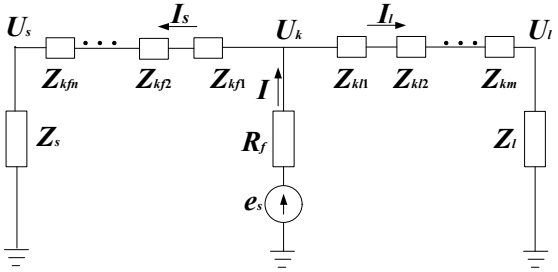

Figure 4. The fault AMV distribution in feeder segments

Z_{kf1}~Z_{kfn} and Z_{kl1}~Z_{klm} are the aerial-mode impedances of the lines between each distribution transformer, denoted as 1, 2, ..., n and 1, 2, ..., m from near to far from the fault point; The AMVs at the fault point, at the beginning and end of the line are U_k, U_s, and U_l.

$$\begin{aligned} U_k &= U_{l1} = (R_{s1} + R_{L1})i_1 + (L_{s1} + L_{L1})\frac{di_1}{dt} \\ U_s &= L_s \frac{di_1}{dt} \\ U_l &= L_l \frac{di_1}{dt} \end{aligned} \tag{5}$$

In Figure 4, the transient voltages U_{f1} and U_{l1} on both sides of the transformer adjacent to the fault point are obtained from Kirchhoff's voltage law (KVL) as follows:

$$\begin{aligned} U_{f1} &= U_k - \frac{Z_{kf1}}{Z_{kfall}} U_s \\ U_{l1} &= U_k - \frac{Z_{kl1}}{Z_{klall}} U_l \end{aligned} \tag{6}$$

It can be inferred that, the U_k value at the fault point is highest, while the transient voltage value gradually decreases as the distance increases on both sides of the fault point along the feeder. The value of transition resistance R_f at the fault point will affect the magnitude of the voltage U_k at the fault point, but will not change the voltage distribution pattern in Figure 4. Since the load aerial-mode impedance Z_l is much greater than the system aerial-mode impedance Z_s, the aerial-mode impedance on both sides of the fault point meets:

$$| Z_s | + | Z_{kf} | = | Z_{kl} | + | Z_l | \tag{7}$$

Therefore, the relevant magnitudes between the AMVs U_k, U_s, and U_l at the fault point, the beginning and end point of the line, can be illustratively shown as the following Figure 5:

 doi:10.20944/preprints202403.1099.v1

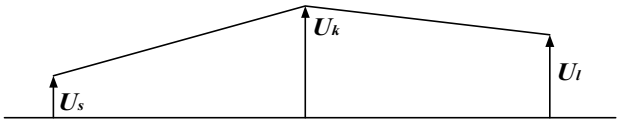

Figure 5. Modulus comparison of the AMVs

The distribution characteristics of AMV is applicable to common grounding system. According to the location of the distribution transformer on the feeder, the magnitude of the AMV signal also follows the similar distribution pattern. At the LV side, the AMV of the fault line is significantly higher than that of other non-fault lines. On the fault line, the AMV at the fault point is higher than other points on its both sides. Based on this, a single-phase grounding fault occurred on the MV side can be detected, and furthermore the fault line and location can be pinpointed.

3. Simulation Result and Analysis

Simulation is carried out using SIMULINK on a system as shown in Figure 6. There are three 10kV feeders *L*1, *L*2 and *L*3 in the system, with multiple distribution transformers. The transformer winding in the substation is DYn, and the neutral point grounding method in 10kV is configurable. Both 10kV lines and LV loads adopt RLC parameter models, and the distribution transformer windings are set as DYn.

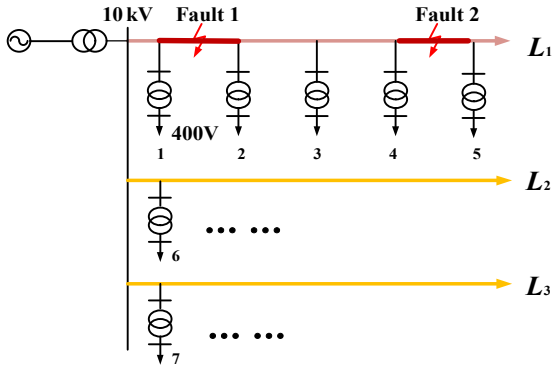

Figure 6. Simulation system diagram

Select *L*1 as the fault line, two single-phase grounding fault scenarios are studied with various neutral grounding modes and grounding resistances. Faults 1 and 2 are located on the primary feeder segment in the middle of distribution transformer 1 and 2, transformer 4 and 5 respectively.

When the neutral point of the system is grounded through the ASC and the fault resistance is 0Ω, assume fault 1 occurs at 0.2s. Figure 7 shows the AMV change in the LV side of the transformers 1-5 on the fault line *L*1, and Figure 8 shows that in the LV side of the transformers 6-7 on the non-fault line *L*2 and *L*3.

Preprints.org (www.preprints.org) | NOT PEER-REVIEWED | Posted: 22 March 2024 doi:10.20944/preprints202403.1099.v1

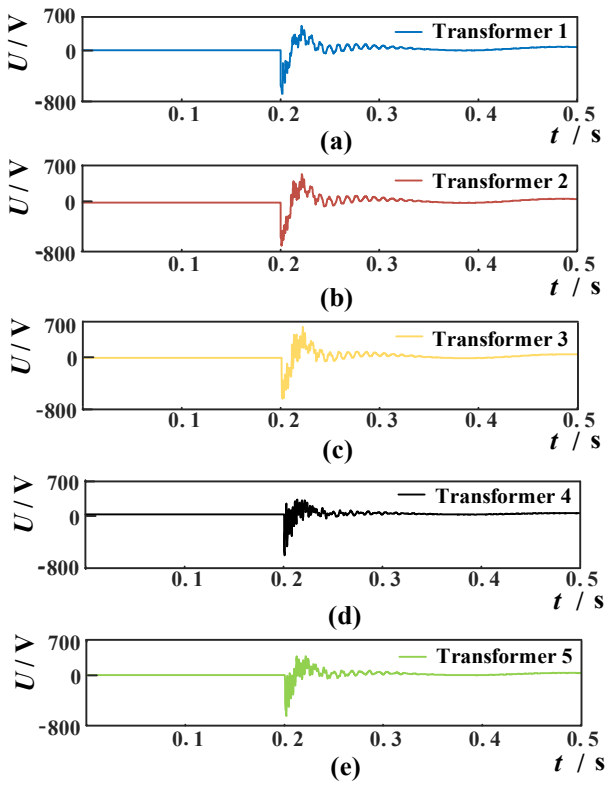

Figure 7. The AMV changes at transformers 1-5 (fault 1).

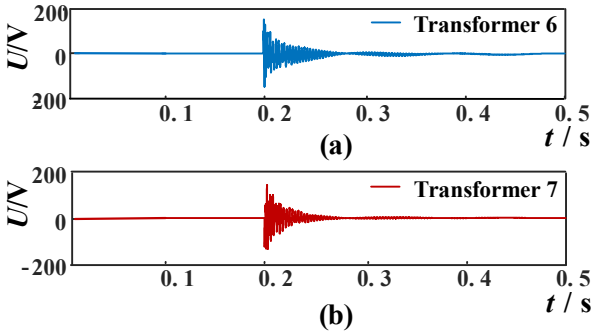

Figure 8. The AMV changes at transformers 6-7 (fault 1).

From Figure 7-8, it can be seen that when the neutral point is grounded through the ASC and the fault resistance is 0Ω, the AMV on the LV side of the fault line shows sharp change after the fault occurrence, and the magnitude of its instantaneous value is significant enough to be reliably detected by practical sensors. Although the AMV on the LV side of the non-fault lines changes as well at the same time, the magnitude of the AMV in the fault line is much larger than that of the non-fault line, and the difference is very noticeable. From amplitude perspective in Table 1, The AMV has a maximum value of 699.7V at transformer 2, and 694.9V at transformer 1, while the results in transformer 3, 4, and 5 are significantly lower. Therefore, based on the comparison of amplitude results, the MV fault section can be judged as locates between transformer 1 and 2. Table 1 also shows simulation results of fault 1 with different neutral grounding modes and grounding resistances.

Table 1. Comparison of Simulation Results of Fault 1.

Neutral grounding mode	Fault resistance/Ω	AMV amplitude /V						
		1	**2**	3	4	5	6	7
Arc	0	**694.9**	**699.7**	686.0	682.3	679.1	126.6	124.2
	10	**575.4**	**577.7**	573.7	570.2	568.0	109.8	108.0

 doi:10.20944/preprints202403.1099.v1

suppression coil	100	**219.7**	**221.4**	217.3	214.8	211.7	36.9	36.1
Ungrounded	0	**913.1**	**920.0**	902.4	889.5	877.5	159.6	161.4
	10	**749.7**	**754.6**	745.5	738.2	730.1	138.7	137.6
	100	**274.9**	**276.7**	271.7	267.6	263.8	66.1	65.7
Resistance 6Ω	0	**759.3**	**765.1**	755.8	746.9	738.6	142.3	141.3
	10	**628.8**	**631.3**	623.3	615.1	609.5	126.8	125.8
	100	**252.0**	**253.8**	249.7	247.1	243.2	56.5	56.1

Table 2 shows the results for fault 2 of all AMVs with different fault resistances and neutral grounding modes. Taking one example, when the neutral point is grounded through the ASC and the fault resistance is 0Ω, and the AMV has a maximum value of 680.6V at transformer 4, and 677.2V at transformer 5, which indicates the MV fault is located between these two transformers.

Table 2. Comparison of Simulation Results of Fault 2

Neutral grounding mode	**Fault resistance/Ω**	**AMV amplitude /V**						
		1	**2**	3	4	5	6	7
Arc suppression coil	0	662.2	667.1	671.7	**680.6**	**677.2**	122.2	124.0
	10	561.9	567.3	563.7	**569.6**	**567.3**	107.6	106.9
	100	204.6	207.7	211.8	**215.1**	**213.4**	35.7	34.4
Ungrounded	0	871.4	883.5	898.6	**912.8**	**907.9**	153.4	161.3
	10	722.3	728.1	733.8	**742.7**	**737.3**	126.6	129.1
	100	253.8	258.4	262.6	**267.3**	**266.4**	64.7	62.3
Resistance 6Ω	0	729.2	736.9	743.6	**751.9**	**748.3**	136.7	135.8
	10	607.3	612.2	619.3	**625.3**	**623.5**	114.4	112.4
	100	231.7	234.8	238.0	**241.5**	**240.8**	54.3	53.1

From the results shown in Table 1 and Table 2, it can be seen that although the AMV magnitude change significantly along with the changing the fault resistance and neutral grounding mode, it follows the distribution pattern as analyzed. Fault line *L*1 can be clearly identified since its distribution transformers have noticeable higher AMV amplitude than transformers on *L*2, *L*3 in all cases. The MV fault location of fault line *L*1 can also be pinpointed by finding its two distribution transformers with highest AMV amplitude, which are transformer 2 and 1 for fault 1, transformer 4 and 5 for fault 2. However, it can be seen that the AMV amplitude in fault segment decreases as the fault grounding resistance increases, which infers a limitation of the proposed method in high impedance fault when the AMV amplitude differences between fault line and non-fault line are not that distinguishable with practical sensor measurements.

4. Lab Experiment Result and Analysis

The proposed method is also tested in lab system shown in Figure 9, in which power supply is provided by a 220kV transformer. There are two 10kV/400V distribution transformers M, N on the 10kV distribution feeder, with RLC adjustable loads simulating transformer loads.

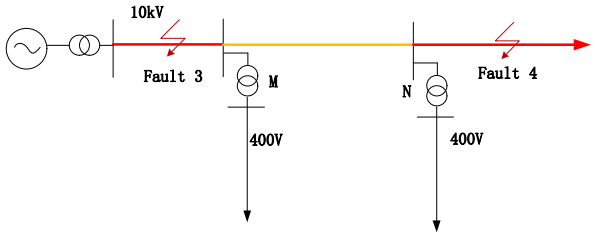

Figure 9. Lab experiment system

 doi:10.20944/preprints202403.1099.v1

The fault 3 is set on 10kV feeder primary upstream of distribution transformer M, and the fault signals are picked up through wave recorder installed at LV side of distribution transformers. When metallic single-phase-to-ground fault is triggered at phase A of the feeder, the neutral point is grounded through ASC, and AMV changes in LV side of distribution transformers are shown in Figure 10.

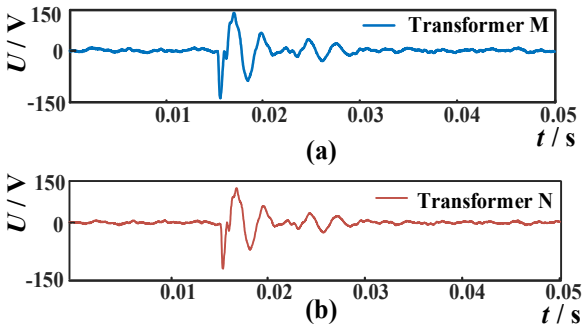

Figure 10. The AMV changes at transformers M, N (fault 3)

Then the fault 4 is set downstream of distribution transformer N while other conditions remain unchanged, and AMV changes in LV side are shown in Figure 11.

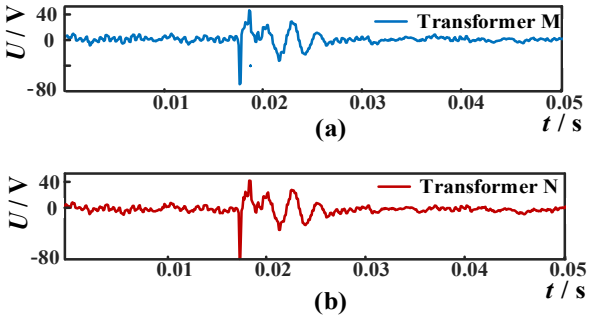

Figure 11. The AMV changes at transformers M, N (fault 4)

Table 3 shows the results of the AMV amplitude for every transformer in fault 3 and fault 4.

Table 3. Comparison of Calculation Results of Fault 3 and Fault 4

	Transformer	Amplitude /V
Fault 3	M	**133.31**
	N	123.78
Fault 4	M	75.50
	N	**78.53**

It can be seen that when the fault point is located upstream of the transformer M (fault 3), the amplitude of the AMV on the LV side of transformer M near the fault point is 144.98V, which is greater than 123.62V at transformer N which is further from the fault point. Similarly, after changing the location of the fault point (fault 4), the amplitude of the AMV in transformer N is 78.73V, which is greater than 69.64V in transformer M. It can also be noted that the fault location change leads to slightly change of AMV. The results conform with the characteristics proving the effectiveness of the proposed method.

Table 4 lists the lab experiment results with different combinations of fault resistances and neutral grounding methods. Constrained by the lab facilities, only two scenarios for the fault resistances (0Ω and 500Ω) are tested. In the test, changing the fault resistance, neutral grounding mode and fault point location leads to the change in AMV amplitude. The results confirm that the amplitude of the AMV near the fault point is significantly larger than that located further away, indicating that effectiveness of the proposed method in locating the MV fault section by comparing

 doi:10.20944/preprints202403.1099.v1

the amplitude of the AMV. However, in the case, with the neutral point grounded through ASC when the fault resistance is 500Ω, although the AMV amplitude at transformer M is still greater than that of transformer N, the amplitude of AMV is too low, which also indicates that limitation of the proposed method for high impedance fault.

Table 4. Lab Experiment Results

Fault 3			
	Neutral grounding mode	**Fault resistance /Ω**	**Amplitude /V**
Transformer M	Arc suppression coil	0	133.31
		500	2.82
	Ungrounded	0	398.14
		500	3.66
	Resistance 6Ω	0	201.2869
		500	3.32
Transformer N	Arc suppression coil	0	123.78
		500	2.65
	Ungrounded	0	240.15
		500	3.39
	Resistance 6Ω	0	184.57
		500	3.13
Fault 4			
	Neutral grounding mode	**Fault resistance /Ω**	**Amplitude /V**
Transformer M	Arc suppression coil	0	75.50
		500	1.54
	Ungrounded	0	129.81
		500	2.43
	Resistance 6Ω	0	136.08
		500	2.97
Transformer N	Arc suppression coil	0	78.53
		500	1.83
	Ungrounded	0	187.91
		500	2.62
	Resistance 6Ω	0	150.17
		500	3.09

5. Discussion

This paper proposed a new method for identifying single-phase-to-ground fault occurred in MV feeder and its location in non-effectively grounded distribution system via analyzing the LV sensor measurements. When the fault occurs, the distribution of transient aerial mode voltage (AMV) follows specific characteristic patterns. The fault line can be identified by comparing the abrupt change value of the AMV at each LV sensor. Next, by finding the position of the maximum value of AMV in each LV sensor on the fault line, the fault section can be pinpointed to section between two adjacent distribution transformers. The proposed method can adapt to different neutral grounding modes, and the efficiency has been verified through simulation and lab experiment, for system with relatively low fault resistance. In systems where LV sensors are deployed, this method can work independently or in combination with MV sensors for fault detection, thus has good prospects for practical applications.

As a new idea for detecting single-phase-to-ground fault in non-effectively grounded system, this paper validates the feasibility of identifying the fault line and the fault section on the MV feeders through transient signals acquired by LV sensors. In the future, more studies will be carried out to further improve the adaptability under high impedance fault conditions.

Author Contributions: Conceptualization, Mingze ZHANG; methodology, Mingze ZHANG; software, Mingze ZHANG and Xinyu GUAN; validation, Mingze ZHANG and Xinyu GUAN; formal analysis, Xinyu GUAN; investigation, Xinyu GUAN; resources, Xin AI; data curation, Mingze ZHANG; writing—original draft preparation, Mingze ZHANG; writing—review and editing, Mingze ZHANG; supervision, Xin AI; funding acquisition, Xin AI. All authors have read and agreed to the published version of the manuscript.

Funding: This research received no external funding.

Acknowledgments: This research was supported by the National Key R&D Program of China (Grant no. 2020YFB0905900).

Conflicts of Interest: The authors declare no conflicts of interest. The funders had no role in the design of the study; in the collection, analyses, or interpretation of data; in the writing of the manuscript; or in the decision to publish the results.

References

1. Cheng, L.; Chen Q. A survey on faulty line selection technology for single-phase grounded transmission line in small current neutral grounded system. *Power System Technology*, **2009**, 33(18), 219-224.
2. Wang, J.; Zhu, Y.; Qin, S. Fault line selection method for small current grounding system based on directional traveling wave energy. *Transactions of China Electrotechnical Society*, **2021**, 36(19), 4085-4096.
3. Wang, X.; Du, H.; Liang, Z.; Guo, L.; Gao, J.; Mostafa K.; Liu, W. Single phase to ground fault location method of overhead line based on magnetic field detection and multi-criteria fusion. *Int J Electr Power Energy Syst*, **2023**, 145, 108699.
4. Li, H.; Chen, J.; Liang, Y., Liao, F.; Wang, G. Effects of imbalance on single-phase to ground fault characteristics in low-resistance grounded systems. *Int J Electr Power Energy Syst*, **2020**, 115, 105504.
5. Yao, H.; Cao, M. *Resonant grounding of power system*. China Electric Power Press: Beijing, 2000.
6. Ren, W.; Xue, Y.; Yang, F.; Xu, B. Modeling and analysis of arc grounding faults in isolated neutral distribution network. *Power System Technology*, **2021**, 45(02), 705-712.
7. Liang, D.; Xu B.; Tang, Y.; Wang, P.; Wang, W. Model and detection method for tree-contract single-phase-to-ground faults on 10kV overhead lines. *Proceeding of the CSEE*, **2021**, 41(15), 5221-5232.
8. Zhang, Z.; Liu, J.; Shao, W.; Wang, Y. Fault line selection using multiple disturbance characteristics of fault phase active grounding in resonant grounded distribution networks. *Int J Electr Power Energy Syst*, **2022**, 138: 107931.
9. Li, L.; Gao, H.; Cong, W.; Yuan, T. Location method of single line-to-ground faults in low-resistance grounded distribution networks based on ratio of zero-sequence admittance. *Int J Electr Power Energy Syst*, **2023**; 146, 108777.
10. Luan, X.; Wu, S.; Jia, C.; Yang, Y.; Zhang, Z.; Luo, X. Fault line selection principle of single-phase-to-ground fault based on improved zero-sequence admittance. *Power System Technology*, **2022**, 46(01), 353-360.
11. Wang, Y.; Liu, J.; Zhang, Z.; Zheng, T.; Ren, S.; Chen, J. A faulty line detection method for single phase-to-ground fault in resonant grounding system with CTs reversely connected. *Int J Electr Power Energy Syst*, **2023**, 147, 108873.
12. Xu, B.; Xue, Y.; Feng, G.; Wang, C. Discussion on several problems of earthing fault protection in distribution. *Automation of Electric Power System*, **2019**, 43(20), 1-7.
13. Liu, J.; Zhang, X.; Shen, W.; Quan, L.; Zhang, Z. Performance testing of single phase to earth fault location for distribution network with neutral point non-effectively grounded systems. *Automation of Electric Power System*, **2018**, 42(01), 138-143.
14. Luo, J.; He, J.; Zhao, H.; Yang, H.; Zhang, J.; Liu, L.; Wang, R. Fault line selection based on zero sequence power direction of transient fundamental frequency in MV network grounded with ARC extinguishing coil. *2006 International Conference on Power System Technology*. Chongqing, China, **2006**, 1-4,
15. Yanru N, Xiangjun Z, Zhanlei L, Kun Y, Pengbo X, Zhan W, Chao Z, Yue H. Faulty feeder detection of single phase-to-ground fault for distribution networks based on improved K-means power angle clustering analysis. *Int J Electr Power Energy Syst*, 2022; 142: 108252.
16. Zeng, X.; Yin, X.; Zhang, Z.; Chen, D. Study for negative sequence current distributing and ground fault protection in middle voltage power systems. *Proceedings of the CSEE*, **2001**, 21(6), 84-89.
17. Griffel D, Leitloff V, Harmand Y. A new deal for safety and quality on MV networks. *IEEE Trans on Power Delivery*, **1997**, 12(4), 1428-1433.
18. Lin,X.; Ke, S.; Gao, Y.; Wang, B.; Liu, P. A selective single-phase-to-ground fault protection for neutral un-effectively grounded systems. *Int J Electr Power Energy Syst*, **2011**, 33(4), 1012-1017.
19. Abdul, G.; Ramana, R. A new wavelet based fault detection, classification and location in transmission lines. *Int J Electr Power Energy Syst*, **2015**, 64, 35-40.
20. Yuan, J.; Jiao, Z. Faulty feeder detection for single phase-to-ground faults in distribution networks based on patch-to-patch CNN and feeder-to-feeder LSTM. *Int J Electr Power Energy Syst*, **2023**, 147, 108909.

 doi:10.20944/preprints202403.1099.v1

21. Vladimir, K.; Andrey, L.; Evgenia, K. Monitoring in 6–35 kV power networks, location of single-phase ground fault and detection of fault feeder. *Int J Electr Power Energy Syst*, **2023**; 152, 109271.
22. Ferreira, K.; Emanuel, A. A noninvasive technique for fault detection and location. *IEEE transactions on power delivery*, **2010**, 25(4), 3024-3034.
23. Jiang, B.; Dong, X.; Shi, S. A method of single phase to ground fault feeder selection based on single phase current traveling wave for distribution lines. *Proceeding of the CSEE*, **2014**, 34(34), 6216-6227.
24. Li, G.; Xue, Y.; Xu, B.; Yang, F. Analysis on arc re-ignition transient characteristics for grounding fault in non-solidly grounding system. *Automation of Electric Power System*, **2020**, 44(11), 189-196.
25. Li, T.; Wang, F.; Zhu, L.; Li, J. A new method of distribution network single-phase ground fault line selection based on the intrinsic mode energy entropy. *Power System Technology*, **2008**, 32(S2), 128-132.
26. Yang, F.; Ren, W.; Shen, Y.; Lei, Y.; Xue, Y.; Xu, B. Transient analysis method and identification of arc grounding faults in petersen coil grounded distribution network. *Proceedings of the CSU-EPSA*, **2021**, 33(04), 23-31.
27. Fang, Y.; Xue, Y.; Song, H., Guan, T.; Yang, F.; Xu, B. Transient energy analysis and faulty feeder identification method of high impedance fault in the resonant grounding system. *Proceeding of the CSEE*, **2018**, 38(19), 5636-5645+5921.
28. Xue, Y.; Xu, B.; Feng, Z.; Li, T. Study on transient directional protection principle for small current grounding fault. *Proceeding of the CSEE*, **2003**, 23(7), 51-56.
29. Xue, Y.; Feng, Z.; Xu, B.; Chen, Y.; Li, J. Research on fault line selection for small current grounding based on transient zero sequence current comparison. *Automation of Electric Power System*, **2003**, 27(9), 48-53.
30. Li, Z.; Ye, Y.; Xiao Ma, X.; Lin, X.; Xu, F.; Wang, C.; Ni, X.; Ding, C. Single-phase-to-ground fault section location in flexible resonant grounding distribution networks using soft open points. *Int J Electr Power Energy Syst*, **2020**; 122, 106198.
31. Sang, Z.; Zhang, H.; Pan, Z. Signal phase grounding fault protection fault protection by injecting currents in ineffective grounding system. *Automation of Electric Power System*, **1996**, 20(2), 11-12.
32. Zeng, X.; Yin, X.; Yu, Y. New method for control and protection relay in a compensated medium voltage distribution net-work based on injecting various frequency current. *Proceeding of the CSEE*, **2000**, 20(1), 29-33.
33. Xu, B. Distribution network relay protection and automation. China Electric Power Press, Beijing, 2017.
34. Ojanguren, I.; Ruiz, N.; Garcia, J. MV high impedance faults detection based on LV measurements. *International Conference on Electricity Distribution* (CIRED), Glasgow, Scotland, 2017.
35. Francinei, L.; Pedro, H.; Jose, M.; Roberto, C.; Marino, P. A voltage-based approach for series high impedance fault detection and location in distribution systems using smart meters. *Energies*, **2019**, 12, 3022.
36. Zhang, Y.; Zhang, S.; Zhang, W.; Xiao, X. Fault section location of a distribution network based on voltage variation of the secondary side of a transformer in the station area. *Power System Protection and Control*, **2022**, 50(16), 23-32.
37. Jia, K.; Ren, Z.; Bi, T.; Yang, Q. Ground fault location using the low-voltage-side recorded data in distribution systems. *IEEE Transactions on Industry Applications*, **2015**, 51(6), 4994-5001.
38. Sture, L. Sensitive earth fault protection for MV distribution system. *CIRED*, 1991.
39. Jie, L.; Tang, K.; Zhang, T.; Zhou, X. Research on ground fault line detection based on phase-frequency characteristics of transient signals. *Power System Protection and Control*, **2009**, 37(3), 50-54.
40. Xue, Y. Earth fault detection based on characteristic transient information in non-solidly earthed network. Xi'an Jiaotong University, **2003**. ph.D. thesis.
41. Xu, B.; Xue, Y.; Li, J.; Cheng, Y. Single phase fault detection technique based on transient current and its application in non-solid grounded network. 2001 *Seventh International Conference on Developments in Power System Protection*, Amsterdam, Netherlands, 2001.141-144.